Differentiated Activities of Decorin and Biglycan in the Progression of Post-Traumatic Osteoarthritis

Biao Han[#1], **Qing Li**[#1], **Chao Wang**[1], **Prashant Chandrasekaran**[1], **Ying Zhou**[2], **Ling Qin**[3], **X. Sherry Liu**[3], **Motomi Enomoto-Iwamoto**[4], **Dehan Kong**[2], **Renato V. Iozzo**[5], **David E. Birk**[6], **Lin Han**[1,*]

[1]School of Biomedical Engineering, Science and Health Systems, Drexel University, Philadelphia, PA 19104, United States

[2]Department of Statistical Sciences, University of Toronto, Toronto, ON M5S 3G3, Canada

[3]McKay Orthopaedic Research Laboratory, Department of Orthopaedic Surgery, Perelman School of Medicine, University of Pennsylvania, Philadelphia, PA 19104, United States

[4]Department of Orthopaedics, School of Medicine, University of Maryland, Baltimore, MD 21201, United States

[5]Department of Pathology, Anatomy, and Cell Biology, Sidney Kimmel Medical College, Thomas Jefferson University, Philadelphia, PA 19107, United States

[6]Department of Molecular Pharmacology and Physiology, Morsani School of Medicine, University of South Florida, Tampa, FL 33612, United States

[#] These authors contributed equally to this work.

Abstract

Objective: To delineate the activities of decorin and biglycan in the progression of post-traumatic osteoarthritis (PTOA).

Design: Three-month-old inducible biglycan (Bgn^{iKO}) and decorin/biglycan compound (Dcn/Bgn^{iKO}) knockout mice were subjected to the destabilization of the medial meniscus (DMM) surgery to induce PTOA. The OA phenotype was evaluated by assessing joint structure and sulfated glycosaminoglycan (sGAG) staining via histology, surface collagen fibril nanostructure

[*]Correspondence and requests for materials should be addressed to: Dr. Lin Han, Phone: (215) 571-3821, Fax: (215) 895-4983, lh535@drexel.edu.

and calcium content via scanning electron microscopy, tissue modulus via atomic force microscopy-nanoindentation, as well as subchondral bone structure and meniscus ossification via micro-computed tomography. Outcomes were compared with previous findings in the inducible decorin (Dcn^{iKO}) knockout mice.

Results: In the DMM model, Bgn^{iKO} mice developed similar degree of OA as the control (0.44 [−0.18 1.05] difference in modified Mankin score), different from the more severe OA phenotype observed in Dcn^{iKO} mice (1.38 [0.91 1.85] difference). Dcn/Bgn^{iKO} mice exhibited similar histological OA phenotype as Dcn^{iKO} mice (1.51 [0.97 2.04] difference versus control), including aggravated loss of sGAGs, salient surface fibrillation and formation of osteophyte. Meanwhile, Dcn/Bgn^{iKO} mice showed further cartilage thinning than Dcn^{iKO} mice, resulting in the exposure of underlying calcified tissues and aberrantly high surface modulus. Bgn^{iKO} and Dcn/Bgn^{iKO} mice developed altered subchondral trabecular bone structure in both Sham and DMM groups, while Dcn^{iKO} and control mice did not.

Conclusion: In PTOA, decorin plays a more crucial role than biglycan in regulating cartilage degeneration, while biglycan is more important in regulating subchondral bone structure. The two have distinct activities and modest synergy in the pathogenesis of PTOA.

Keywords

post-traumatic osteoarthritis; decorin; biglycan; proteoglycan; extracellular matrix; murine models

INTRODUCTION

Decorin and biglycan are the two most abundant small proteoglycans present in the extracellular matrix (ECM) of articular cartilage[1]. Classified as class I small leucine-rich proteoglycan (SLRP), decorin and biglycan have highly similar structure, with ≈ 57% homology along their leucine-rich, horseshoe-shaped protein cores[2]. Decorin has one chondroitin sulfate/dermatan sulfate glycosaminoglycan (CS/DS-GAG) chain attached to its N-terminus, while biglycan has two[2]. Given their similarities, the two SLRPs share many activities in their interactions with other matrix molecules, growth factors and cell surface receptors[3]. In fibrous tissues such as tendon and cornea, both decorin and biglycan regulate the matrix collagen fibril assembly[4] and cell signaling[5], where their activities can be compensatory and synergistic[6,7]. In cartilage, decorin is present in both the pericellular matrix (PCM) and further-removed territorial/interterritorial extracellular matrix (T/IT-ECM)[8], while biglycan is localized in the PCM[9]. Such differentiated distributions indicate that they may have distinct activities in cartilage. To this day, although the importance of the two SLRPs in cartilage function and pathology has been well recognized[10], it is unclear how decorin and biglycan individually or synergistically regulate the initiation and progression of osteoarthritis (OA)[11], the most prevalent musculoskeletal disease characterized by the irreversible breakdown of cartilage.

In human cartilage, both decorin and biglycan are significantly up-regulated in OA[12-14]. This up-regulation is hypothesized to be chondrocytes' compensatory attempt to attenuate cartilage degeneration[11]. This hypothesis is supported by our recent finding that decorin functions as a "physical linker" to increase the molecular adhesion of aggrecan, thereby

increasing the integrity of aggrecan networks in normal cartilage ECM[8], and slowing the loss of fragmented aggrecan from degenerative cartilage[15]. This role is supported by the more severe OA phenotype developed in decorin-null ($Dcn^{-/-}$) mice[16] relative to the wild-type (WT) when subjected to the destabilization of the medial meniscus (DMM) surgery[15]. It also explains why, despite its up-regulation in OA cartilage, decorin is not released to the synovial fluid at an increasing level, contrary to the case of biglycan[17]. To this day, it is unclear if biglycan also plays an active role in the progression of OA, and if the two SLRPs have synergistic activities.

This study sought to delineate the individual roles of decorin and biglycan in the progression of post-traumatic osteoarthritis (PTOA), and to elucidate if they have synergistic and/or additive activities. We focus on their activities in PTOA, because it is the most prevalent form of OA in young adults, and leads to long term detrimental influence on the quality of life[18]. Following our recent study on the inducible decorin knockout mice[8,15], we applied the DMM surgery to the inducible biglycan knockout and decorin/biglycan compound knockout murine models[19]. In these mice, we allowed for normal joint growth to maturity, and induced the knockout of each or both SLRPs at the time of DMM. The resulted phenotype thus represented the impact of loss of SLRPs during DMM-induced cartilage remodeling, with pre-deposited developmental defects of cartilage being minimized. In these models, we studied the progression of OA by assessing the morphology, sulfated GAG (sGAG) staining, modulus, fibrillar structure and surface calcium content of cartilage, as well as the structure of subchondral bone and meniscal ossicles.

METHODS

Animal models.

Decorin, biglycan and decorin/biglycan-compound inducible knockout mice ($Dcn^{flox/flox}/Rosa26Cre^{ER}$, $Bgn^{flox/0}/Rosa26Cre^{ER}$ and $Dcn^{flox/flox}/Bgn^{flox/0}/Rosa26Cre^{ER}$, or Dcn^{iKO}, Bgn^{iKO} and Dcn/Bgn^{iKO}) in the C57BL/6 strain were generated as previously described[19], and were housed in the Calhoun animal facility at Drexel University. To induce the knockout of SLRP genes, three consecutive daily intraperitoneal (i.p.) injections of tamoxifen were applied at a dosage of 3 mg/40 g body weight in the form of 20 mg/ml suspended in sesame oil (S3547, Sigma) with 1% volume/volume benzyl alcohol (305197, Sigma) at 3 months of age (first injection started at one week before DMM). Quantitative polymerase chain reaction (qPCR) was performed on femoral head cartilage at day 5 to confirm the tamoxifen-induced gene excision of Dcn and/or Bgn, and to detect any compensatory up-regulation between the two genes (Primers: Dcn, forward: 5'-TGAGCTTCAACAGCATCACC-3', reverse: 5'-AAGTCATTTTGCCCAACTGC-3'; Bgn, forward: 5'-CTACGCCCTGGTCTTGGTAA-3', reverse: 5'-ACTTTGCGGATACGGTTGTC-3'). Control mice include those with normal expressions of decorin and biglycan, including the inducible knockout mice of decorin, or biglycan, or compound injected with vehicle (the same amount of sesame oil and benzyl alcohol but without tamoxifen), and WT mice injected with tamoxifen at the same dose and frequency. All the mice used here were genotyped, following standard procedures[19]. Animal work was approved by the Institutional Animal Care and Use Committee at Drexel University.

The DMM surgery was performed on the right hind knees of skeletally mature, 3-month-old male mice, following the established procedure[20]. Briefly, after anesthesia, the joint capsule was opened and medial meniscotibial ligament was cut to destabilize the medial meniscus. Sham surgery was performed on the contralateral left knee by opening the joint capsule in the same fashion to expose the ligament, but without further damage. Mice were euthanized at 8 weeks after surgery for further analyses ($n = 11$, except $n = 19$ for the control). In our recent study, Dcn^{iKO} and control mice were subjected to the same DMM model, and analyzed following the same paradigm by the same researchers (BH, QL, CW) as the current study[15]. These results were thus analyzed together with Bgn^{iKO}, Dcn/Bgn^{iKO} and additional control mice.

Histology and immunofluorescence imaging.

Whole hind knee joints ($n = 6$, except $n = 10$ for the control) were harvested and fixed in 4% paraformaldehyde, first used for μCT analysis, and then, decalcified in 10% EDTA for 4 weeks, and embedded in paraffin. Serial 6-μm-thick sagittal sections were prepared, and two sections with every consecutive six sections of the medial side of the Sham and DMM knees were stained with Safranin-O/Fast Green, following the established procedure[15]. For each joint, approximately 15 sections were obtained and scored by two blinded observers (QL and CW) using the modified Mankin method[21]. Each section was assigned a score based on the sum of cartilage structure (0-5), chondrocytes (0-3), Safranin-O staining (0-5) and tidemark (0-1). The score of each knee was taken as the maximum of all scored sections[22]. Thicknesses of uncalcified and total cartilage were determined by averaging six values evenly distributed across the entire cartilage in the load bearing medial region.

To validate the reduction of decorin and biglycan by tamoxifen injection at the protein level, immunofluorescence (IF) imaging was performed. Additional paraffin sections were treated with 0.1% pepsin (P7000, Sigma) for antigen retrieval, and blocked with 5% BSA in PBS for 1 hour at room temperature. Sections were first incubated with primary antibody (decorin, LF-114, biglycan, LF-159, Kerafast, 1:100 dilution) overnight at 4°C, and then, with secondary antibody (AlexaFluor 594, ThermoFisher, 1:500) for 2 hours at room temperature ($n = 4$). Sections were washed with PBS, counter-stained, mounted with DAPI (Fluoromount-G, 0100-20, SouthernBiotech), and imaged with a Carl Zeiss Axio Observer Microscope.

AFM-based nanoindentation

AFM-based nanoindentation was applied to freshly dissected femoral condyle cartilage ($n = 5$, except $n = 9$ for the control), using custom-made polystyrene microspherical colloidal tips ($R \approx 5$ μm, nominal $k \approx 8.9$ N/m, HQ:NSC35/Tipless/Cr-Au, cantilever A, NanoAndMore) and a Dimension Icon AFM (BrukerNano) at 10 μm/s indentation rate up to a maximum load of ≈ 1 μN in $1 \times$ PBS with protease inhibitors (Pierce 88266, ThermoFisher). Following the established procedure[23], at least 10-15 locations were tested on each joint to account for spatial heterogeneity. The indentation modulus, E_{ind}, of each location was calculated by fitting the entire loading portion of each force-indentation depth (F-D) curve with the Hertz model, and the average value from each joint was taken as one biological repeat.

Scanning electron microscopy

Scanning electron microscopy (SEM) was applied to quantify the fibril diameter and alignment on the load-bearing region of medial condyle cartilage surfaces ($n = 4$), following the established procedure[24]. Immediately after AFM-nanoindentation, condyle cartilage joints were processed for proteoglycan removal, fixed, dehydrated, air dried overnight, coated with ≈ 6 nm thick platinum-palladium mixture, and then, imaged via a Supra 50 VP SEM (Carl Zeiss). Collagen fibril diameter d_{col}, and alignment angle, θ, were measured using ImageJ. Values of θ were fitted with von Mises probability density function to calculate the von Mises concentration parameter, κ, a quantitative measure of fibril alignment[25], following the established procedure[26]. In addition, since one major distinction between the calcified versus uncalcified cartilage layers is the presence of higher calcium content, we applied SEM with the Energy Dispersive X-ray Spectroscopy (SEM/EDS) to assess the weight percentage of calcium on cartilage surface, which is an indicator of the exposure of underlying calcified layer.

Micro-computed tomography

Micro-computed tomography (μCT) scanning was performed to assess concurrent changes of subchondral bone and meniscus ossification after DMM. For mice purposed for histology, prior to demineralization, knee joints ($n = 5$) were scanned ex vivo using MicroCT 35 (Scanco Medical AG) at 6 μm isotropic voxel size and smoothed by a Gaussian filter (sigma = 1.2, support = 2.0). Following the established procedure[27,28], we estimated the thickness of subchondral bone plate (SBP.Th), the bone volume fraction (BV/TV), trabecular number (Tb.N), and trabecular thickness (Tb.Th) of subchondral trabecular bone (STB) on the central load-bearing region of medial tibial plateau, as well as meniscal ossicle volume and osteophyte formation on the medial side.

Statistical analysis

Linear mixed effect model was applied to test quantitative outcomes including Mankin score, cartilage thickness, E_{ind}, d_{col}, calcium content and μCT outcomes using the R package lme4 (version 1.1-19)[29]. In all the tests, genotype, surgery type, and position (anterior versus posterior for meniscal ossicle volume) were treated as fixed effect factors when applicable, with interaction terms between genotype and surgery, or between genotype and position. Individual animal effect was treated as a randomized factor, and surgery type and position were considered as within-subject factors. Prior to the test, Shapiro-Wilk test was applied to residuals to confirm that these outcomes did not deviate significantly from normal distribution, and likelihood ratio test was applied to determine the choice of two covariance structures, unstructured versus compound symmetry. For all comparisons, p-values were adjusted for family-wise type I errors via Tukey-Kramer test between genotypes for each surgery type, and via Holm-Bonferroni correction for multi-contrasts between surgeries or between positions across multiple genotypes. For fibril orientation data, Mardia and Jupp test of concentration equality[25] was applied to compare the von Mises concentration κ between genotypes and surgery types, followed by the Holm-Bonferroni correction. All quantitative and statistical outcomes were summarized in Tables S1-S5.

RESULTS

Reduction of decorin and biglycan expressions in the induced knockout models.

In all inducible knockout models, daily injection of tamoxifen for 3 days substantially reduced the expressions of each or both SLRPs by day 5. In single knockout mice, we did not notice the up-regulation of biglycan in response to the loss of decorin, and vice versa, illustrating limited compensatory effects (Fig. 1a). In alignment with gene expression results, IF imaging also showed marked reduction in the staining of decorin in Dcn^{iKO} and Dcn/Bgn^{iKO} cartilage (Fig. 1b), and biglycan in Bgn^{iKO} and Dcn/Bgn^{iKO} groups (Fig. 1c), in both Sham and DMM knees following the tamoxifen injection. In control mice, we detected increased staining of decorin, but not biglycan, after DMM (Fig. 1b,c), consistent with our previous observations on WT mice[15,30]. In comparison to the control, Dcn^{iKO} and Bgn^{iKO} mice showed similar staining patterns of biglycan and decorin, respectively. Also, in Dcn^{iKO} mice, biglycan remained to be localized in the PCM after DMM. These results supported limited compensatory effects, corroborating the qPCR results. Thus, we validated these murine models for studying the impact of the loss of individual or both SLRPs on DMM-induced PTOA.

Impacts of decorin and biglycan on the degradation of cartilage after DMM.

By 8 weeks after DMM, all four genotypes exhibited salient histological signs of OA, including reduced sGAG staining, surface fissures, increased chondrocyte hypertrophy and cartilage thinning (reduced $t_{uncalcified}$ and t_{total}), contributing to increased modified Mankin scores (Fig. 2). Amongst the genotypes, Bgn^{iKO} (6.22 [5.68 6.76] Mankin score, mean [95% CI]) did not show appreciable differences relative to the control post-DMM (5.78 [5.35 6.21], 0.44 [−0.18 1.05] difference, $p = 0.273$) (Fig. 2a,b). This was distinct from the more severe OA observed in Dcn^{iKO} mice (7.17 [6.89 7.44], 1.38 [0.91 1.85] difference versus control). Thus, loss of biglycan had a lesser impact on DMM-induced cartilage degeneration than the loss of decorin.

In Dcn/Bgn^{iKO} mice, the Mankin score (7.29 [6.87 7.71]) was higher than that of control (1.51 [0.97 2.04] difference) and Bgn^{iKO} (1.07 [0.47 1.67] difference) mice, but similar to that of Dcn^{iKO} mice (0.13 [−0.32 0.57] difference, Fig. 2b). On the other hand, Dcn/Bgn^{iKO} mice developed lower uncalcified cartilage thickness, $t_{uncalcified}$ (16.4 [14.0 18.9] μm), compared to Dcn^{iKO} mice (24.4 [21. 6 27.2] μm, 8.0 [4.7 11.2] μm difference, Fig. 2c). This further reduction, however, did not lead to higher Mankin scores, as cartilage erosion has not extended into the calcified cartilage layer in both genotypes, yielding similar scores on cartilage structure. Thus, upon the loss of decorin, the concomitant loss of biglycan did not markedly aggravate the progression of OA based on histological analysis. In the Sham group, unlike the single knockout mice, Dcn/Bgn^{iKO} mice showed mild Mankin scores (2.17 [1.62 2.71]) and reduced cartilage thickness (Fig. 2b-d), indicating a modest impact of concomitant loss of decorin and biglycan on cartilage post-natal maintenance.

Impacts of decorin and biglycan on cartilage surface fibrillar structure and modulus after DMM.

In healthy joints, cartilage surface is characterized by transversely random mesh of collagen fibrils[8], as present in all Sham groups and the DMM groups of control and Bgn^{iKO} mice (Fig. 3a). In contrast, both Dcn^{iKO} and Dcn/Bgn^{iKO} cartilage surfaces developed highly aligned collagen fibrils along the mediolateral orientation, that is, the direction subjected to extensive shearing by the destabilized medial meniscus. These changes were signified by the higher von Mises concentration, κ, indicating salient surface fibrillation (Fig. 4a). Meanwhile, we did not notice significant changes in average surface fibril diameter, d_{col}, amongst the four genotypes, or between Sham and DMM groups (Fig. 4b).

The EDS analysis did not detect appreciable calcium content in all Sham groups (data not shown). In DMM groups, low calcium content was detected on control, Dcn^{iKO} and Bgn^{iKO} cartilage surfaces (0.5% wt.), as expected for uncalcified cartilage. The surface of Dcn/Bgn^{iKO} cartilage, however, showed significantly higher calcium amount (1.08 [0.59 1.56]% wt., $n = 6$, Fig. 5a). This concentration was much lower than the calcium content in bone ($\approx 26.6\%$ wt. based on 67% dry weight of hydroxyapatite in bone[31]), affirming the histological finding that cartilage has not undergone full erosion by 8 weeks. This observation suggested that the underlying calcified cartilage has started to be partially exposed, which was not yet detectable by histology, but apparent at the nanoscale.

In Dcn^{iKO}, Bgn^{iKO} and control mice, the DMM group showed significantly lower modulus, E_{ind}, than the Sham group (Fig. 5b), illustrating impaired cartilage load-bearing function in OA. In Dcn/Bgn^{iKO} mice, however, we observed much higher modulus than other genotypes after DMM. This finding can be explained by the partial exposure of the stiffer calcified layer, as evidenced by the higher calcium content (Fig. 5a). This aberrantly high modulus does not represent the restoration of cartilage biomechanical function, but rather, is an indicator of salient cartilage erosion, and thus, represents more severe cartilage damage[23]. Taken together, despite not having higher Mankin scores than Dcn^{iKO} mice after DMM (Fig. 2b), Dcn/Bgn^{iKO} mice exhibited more severe cartilage damage, as signified by lower $t_{uncalcified}$ (Fig. 2c), higher calcium content (Fig. 5a) and aberrantly high surface modulus (Fig. 5b).

Altered subchondral bone structure with the loss of biglycan.

For the control mice, by 8 weeks after DMM, we did not detect significant changes in subchondral bone plate (SBP) or subchondral trabecular bone (STB) structure, except for a mild increase in STB Tb.N (Fig. 6a-e). This is in agreement with literature showing that in the DMM model, subchondral bone changes only occur after full erosion of cartilage in late OA[32]. Comparing the four genotypes, we did not notice significant differences between the control and Dcn^{iKO} mice for both surgery groups (Fig. 6a-e). Bgn^{iKO} and Dcn/Bgn mice, however, developed significantly altered STB structure relative to the control and Dcn^{iKO} mice, marked by decreased BV/TV, Tb.N and Tb.Th, for both surgery groups. In contrast, we detected the formation of osteophytes, another sign of more advanced OA[33], in Dcn^{iKO} and Dcn/Bgn^{iKO} joints, but not in control or Bgn^{iKO} joints (Fig. 7a). At both the anterior and posterior horns of the meniscus, all four genotypes showed increased ossification after

DMM, and this increased ossification was similar amongst all genotypes (Fig. 7b,c). Collectively, findings from µCT suggested that biglycan has a more direct impact on subchondral bone remodeling, while decorin has a more important role in OA.

DISCUSSION

Differentiated activities of decorin and biglycan in DMM-induced PTOA.

This study highlights the differentiated activities of decorin and biglycan in the progression of DMM-induced PTOA. In degenerative cartilage, decorin functions as a "physical linker" to increase the retention of fragmented aggrecan, thereby slowing aggrecan loss[15]. In the DMM model, loss of decorin leads to accelerated sGAG depletion, cartilage fibrillation, and thus, more severe OA[15], while loss of biglycan does not have a marked impact on cartilage degradation or OA progression (Fig. 2). Such contrast can be attributed to differences in their distribution, binding activities, as well as response to DMM and inflammation. In healthy cartilage, biglycan shows much higher binding affinity than decorin to PCM-specific molecules, such as collagen VI and matrilins[34,35], which may contribute to its localization in the PCM. Thus, unlike decorin, biglycan possibly primarily regulates the integrity of PCM, not the ECM as a whole. Also, different from decorin, biglycan does not undergo salient changes in its concentration or distribution after DMM (Fig. 1b)[30]. This corroborates observations in bovine[36] and murine[15] cartilage explant models, in which, stimulation by inflammatory cytokine IL-1β increases the expression of decorin, but not biglycan. Thus, although biglycan may be crucial to the integrity of cartilage PCM, and may mediate the canonical Wnt signaling of chondrocytes[37], its activities are not markedly altered or stimulated by DMM, indicating that biglycan may not be an essential player in OA pathogenesis in the DMM PTOA model.

In both Sham and DMM groups, loss of biglycan alters the structure of subchondral trabecular bone, while loss of decorin does not (Fig. 6). This is consistent with literature showing that biglycan plays a more crucial role than decorin in regulating bone homeostasis and remodeling[38-41]. Despite these changes in subchondral bone, Bgn^{iKO} mice do not show altered cartilage degradation (Figs. 2, 3), suggesting limited cross-talk between subchondral bone remodeling and cartilage degradation in DMM-induced OA. Furthermore, the observation that the Sham and DMM knees of Bgn^{iKO} mice have similar subchondral bone structure (Fig. 6) suggests that the regulation of subchondral bone by biglycan does not directly influence the pathogenesis of DMM-induced OA, and vice versa.

Our results do not rule out a potential critical role of biglycan in more advanced PTOA or other forms of OA. In late stage human OA, biglycan is up-regulated, undergoes substantial fragmentation and has an increased presence in the T/IT-ECM[13,14]. Also, in late OA, unlike the case of decorin, an increasing amount of soluble, fragmented biglycan is released to the synovial fluid, which may accelerate sGAG loss through elevating NF-κB activities[17]. This potential adverse effect of biglycan is not observed here, as by 8 weeks after DMM, the PCM has not yet lost its distinction to the bulk ECM[30], and biglycan remains to be sequestered within the PCM (Fig. 1b). It is possible that, at a more advanced stage, when biglycan fragments are released from the damaged PCM, biglycan could become an important player in OA pathogenesis. In addition, both decorin and biglycan could have

different activities in other forms of OA. For example, $Dcn^{-/-}$ mice demonstrated higher resistance to forced running-induced OA[42], which can be attributed to different OA etiology in the over-exercised OA model[8,15]. Also, $Bgn^{-/-}$ mice develop accelerated OA during aging[43], illustrating a potential role of biglycan in overall cartilage health and spontaneous OA.

Modest synergy between decorin and biglycan in DMM-induced PTOA.

In the DMM model, Dcn/Bgn^{iKO} mice develop similar Mankin score (Fig. 2b), surface fibrillation (Figs. 3b and 4a) and osteophyte formation (Fig. 7a) as Dcn^{iKO} mice, but show accelerated cartilage thinning (Fig. 2c, d), higher surface calcium content (Fig. 5a) and aberrantly higher surface modulus (Fig. 5b). These results illustrate a moderately higher degree of cartilage damage in Dcn/Bgn^{iKO} mice. This modest synergy between the two SLRPs could be due to their coordinated impacts on the PCM integrity. In cartilage, the PCM plays a crucial role in modulating cell-ECM interactions and chondrocyte mechanotransduction[44]. Degradation of the PCM, and associated alteration of chondrocyte mechanotransduction are among the earliest events that precede the initiation of PTOA[30]. Loss of decorin is expected to aggravate the degradation of PCM by accelerating the depletion of fragmented aggrecan[15], which may accelerate the disruption of chondrocyte mechanotransduction[45]. Concomitant loss of biglycan, a crucial PCM constituent, could further accelerate the PCM disruption, and thus, impair chondrocyte mechanotransduction and exacerbate cartilage degradation. Meanwhile, Dcn/Bgn^{iKO} mice develop similar subchondral bone changes as Bgn^{iKO} mice (Fig. 6b-e), illustrating limited synergy of the two SLRPs in subchondral bone remodeling. Our future studies will thus focus on the activities of the two SLRPs in advanced OA, in which, they may show stronger synergy in regulating chondrocyte mechanobiology and cartilage degradation.

On the technical front, our study highlights the importance of assessing cartilage degradation beyond the scope of standard histological analysis. By 8 weeks after DMM, mice develop moderate OA, and the four genotypes only exhibit modest differences in Mankin scores (Fig. 2b). However, results from SEM, AFM and μCT analyses show clear signs of more advanced OA in Dcn^{iKO} and Dcn/Bgn^{iKO} mice, including surface fibrillation, exposure of calcified cartilage and formation of osteophytes. Therefore, integrating histology with more focused structural and biomechanical tools can provide a more sensitive and in-depth assessment of OA etiology and cartilage damage.

Comparison of decorin and biglycan activities in other connective tissues.

The limited compensation and synergy of decorin and biglycan in cartilage is in stark contrast to their activities in fibrous tissues such as tendon and cornea, in which, they share similar roles of regulating the assembly of collagen fibrils[4]. In cornea, biglycan is up-regulated in the deficiency of decorin, but not vice versa, whereas their compound loss leads to more severe defects in collagen fibril nanostructure in $Dcn^{-/-}/Bgn^{-/-}$ mice[6]. A similar compensatory pattern is observed in the flexor digitorum longus (FDL) tendon of juvenile $Dcn^{-/-}$ mice at 1 month of age[7], but not in the patellar tendon of old Dcn^{iKO} mice at 16 months of age[46]. In aged tendon, the compound induced knockout of decorin and biglycan also does not result in more severe biomechanical changes than single knockouts.[46]

In the knee joint, biglycan has shown synergistic activities with other SLRPs, including fibromodulin, a class II SLRP, and epiphycan, a class III SLRP. Both $Bgn^{-/-}/Fmod^{-/-}$[47] and $Bgn^{-/-}/Epn^{-/-}$[43] mice develop more severe spontaneous OA than the respective single knockouts. Given that biglycan has the highest structural homology with decorin[2], our ongoing work aims to query the potential synergy of the two in more advanced PTOA and aging-associated spontaneous OA. In particular, aging of cartilage is associated with reduced chondrocyte autophagy[48]. Decorin and biglycan can both evoke autophagy in other cell types[49,50], we will study their roles in regulating the autophagy of chondrocytes.

CONCLUSIONS

In summary, decorin and biglycan have differentiated activities in the progression of early-to-intermediate PTOA. Unlike decorin, biglycan does not play a major role in regulating cartilage degradation in DMM-induced PTOA, and the compound loss of both SLRPs shows modest synergistic impacts. While decorin is more crucial in regulating cartilage integrity, biglycan has a stronger impact on subchondral bone structure. These observations are distinct from the highly coordinated activities of the two SLRPs in fibrous tissues. Therefore, decorin, rather than biglycan, could serve as a potential target for developing effective intervention strategies for attenuating the progression of PTOA.

Supplementary Material

Refer to Web version on PubMed Central for supplementary material.

Acknowledgment

References

1. Poole AR, Rosenberg LC, Reiner A, Ionescu M, Bogoch E, Roughley PJ. Contents and distributions of the proteoglycans decorin and biglycan in normal and osteoarthritic human articular cartilage. J. Orthop. Res 1996;14:681–689. [PubMed: 8893759]

2. Iozzo RV. Matrix proteoglycans: from molecular design to cellular function. Annu. Rev. Biochem 1998;67:609–652. [PubMed: 9759499]

3. Iozzo RV, Goldoni S, Berendsen AD, Young MF. Small leucine-rich proteoglycans. In: The Extracellular Matrix: an Overview, Mecham RF Ed. Berlin: Springer-Verlag. 2011:197–231.

4. Chen S, Birk DE. The regulatory roles of small leucine-rich proteoglycans in extracellular matrix assembly. FEBS J. 2013;280:2120–2137. [PubMed: 23331954]

5. Schaefer L, Iozzo RV. Biological functions of the small leucine-rich proteoglycans: from genetics to signal transduction. J. Biol. Chem 2008;283:21305–21309. [PubMed: 18463092]

6. Zhang G, Chen S, Goldoni S, Calder BW, Simpson HC, Owens RT, McQuillan DJ, Young MF, Iozzo RV, Birk DE. Genetic evidence for the coordinated regulation of collagen fibrillogenesis in the cornea by decorin and biglycan. J. Biol. Chem 2009;284:8879–8888.

7. Zhang G, Ezura Y, Chervoneva I, Robinson PS, Beason DP, Carine ET, Soslowsky LJ, Iozzo RV, Birk DE. Decorin regulates assembly of collagen fibrils and acquisition of biomechanical properties during tendon development. J. Cell. Biochem 2006;98:1436–1449. [PubMed: 16518859]

8. Han B, Li Q, Wang C, Patel P, Adams SM, Doyran B, Nia HT, Oftadeh R, Zhou S, Li CY, Liu XS, Lu XL, Enomoto-Iwamoto M, Qin L, Mauck RL, Iozzo RV, Birk DE, Han L. Decorin regulates the

aggrecan network integrity and biomechanical functions of cartilage extracellular matrix. ACS Nano 2019;13:11320–11333. [PubMed: 31550133]

9. Kavanagh E, Ashhurst DE. Development and aging of the articular cartilage of the rabbit knee joint: distribution of biglycan, decorin, and matrilin-1. J. Histochem. Cytochem 1999;47:1603–1616. [PubMed: 10567444]

10. Heinegård D. Proteoglycans and more – from molecules to biology. Int. J. Exp. Pathol 2009;90:575–586. [PubMed: 19958398]

11. Ni GX, Li Z, Zhou YZ. The role of small leucine-rich proteoglycans in osteoarthritis pathogenesis. Osteoarthritis Cartilage 2014;22:896–903. [PubMed: 24795272]

12. Cs-Szabó G, Roughley PJ, Plaas AHK, Glant TT. Large and small proteoglycans of osteoarthritic and rheumatoid articular-cartilage. Arthritis Rheum. 1995;38:660–668. [PubMed: 7538297]

13. Bock HC, Michaeli P, Bode C, Schultz W, Kresse H, Herken R, Miosge N. The small proteoglycans decorin and biglycan in human articular cartilage of late-stage osteoarthritis. Osteoarthritis Cartilage 2001;9:654–663. [PubMed: 11597178]

14. Melrose J, Fuller ES, Roughley PJ, Smith MM, Kerr B, Hughes CE, Caterson B, Little CB. Fragmentation of decorin, biglycan, lumican and keratocan is elevated in degenerate human meniscus, knee and hip articular cartilages compared with age-matched macroscopically normal and control tissues. Arthritis Res. Ther 2008;10:R79. [PubMed: 18620607]

15. Li Q, Han B, Wang C, Tong W, Tseng WJ, Han L-H, Liu XS, Enomoto-Iwamoto M, Mauck RL, Qin L, Iozzo RV, Birk DE, Han L. Mediation of cartilage matrix degeneration and fibrillation by decorin in post-traumatic osteoarthritis. Arthritis Rheumatol. 2020;72:1266–1277. [PubMed: 32162789]

16. Danielson KG, Baribault H, Holmes DF, Graham H, Kadler KE, Iozzo RV. Targeted disruption of decorin leads to abnormal collagen fibril morphology and skin fragility. J. Cell Biol 1997;136:729–743. [PubMed: 9024701]

17. Barreto G, Soininen A, Ylinen P, Sandelin J, Konttinen YT, Nordstrom DC, Eklund KK. Soluble biglycan: a potential mediator of cartilage degradation in osteoarthritis. Arthritis Res. Ther 2015;17:379. [PubMed: 26703441]

18. Helmick CG, Felson DT, Lawrence RC, Gabriel S, Hirsch R, Kwoh CK, Liang MH, Kremers HM, Mayes MD, Merkel PA, Pillemer SR, Reveille JD, Stone JH. Estimates of the prevalence of arthritis and other rheumatic conditions in the United States. Part I. Arthritis Rheum. 2008;58:15–25. [PubMed: 18163481]

19. Robinson KA, Sun M, Barnum CE, Weiss SN, Huegel J, Shetye SS, Lin L, Saez D, Adams SM, Iozzo RV, Soslowsky LJ, Birk DE. Decorin and biglycan are necessary for maintaining collagen fibril structure, fiber realignment, and mechanical properties of mature tendons. Matrix Biol. 2017;64:81–93. [PubMed: 28882761]

20. Glasson SS, Blanchet TJ, Morris EA. The surgical destabilization of the medial meniscus (DMM) model of osteoarthritis in the 129/SvEv mouse. Osteoarthritis Cartilage 2007;15:1061–1069. [PubMed: 17470400]

21. McNulty MA, Loeser RF, Davey C, Callahan MF, Ferguson CM, Carlson CS. Histopathology of naturally occurring and surgically induced osteoarthritis in mice. Osteoarthritis Cartilage 2012;20:949–956. [PubMed: 22595226]

22. Zhang X, Zhu J, Liu F, Li Y, Chandra A, Levin LS, Beier F, Enomoto-Iwamoto M, Qin L. Reduced EGFR signaling enhances cartilage destruction in a mouse osteoarthritis model. Bone Res. 2014;2:14015. [PubMed: 26120493]

23. Doyran B, Tong W, Li Q, Jia H, Zhang X, Chen C, Enomoto-Iwamoto M, Lu XL, Qin L, Han L. Nanoindentation modulus of murine cartilage: a sensitive indicator of the initiation and progression of post-traumatic osteoarthritis. Osteoarthritis Cartilage 2017;25:108–117. [PubMed: 27568574]

24. Wang C, Brisson BK, Terajima M, Li Q, Hoxha K, Han B, Goldberg AM, Liu XS, Marcolongo MS, Enomoto-Iwamoto M, Yamauchi M, Volk SW, Han L. Type III collagen is a key regulator of the collagen fibrillar structure and biomechanics of articular cartilage and meniscus. Matrix Biol. 2020;85-86:47–67. [PubMed: 31655293]

25. Mardia KV, Jupp PE. Tests of von Mises distributions. In: Directional Statistics London, UK: John Wiley & Sons, Ltd. 2000:119–143.

26. Li Q, Qu F, Han B, Wang C, Li H, Mauck RL, Han L. Micromechanical anisotropy and heterogeneity of the meniscus extracellular matrix. Acta Biomater. 2017;54:356–366. [PubMed: 28242455]

27. Huang H, Skelly JD, Ayers DC, Song J. Age-dependent changes in the articular cartilage and subchondral bone of C57BL/6 mice after surgical destabilization of medial meniscus. Sci. Rep 2017;7:42294. [PubMed: 28181577]

28. Moodie JP, Stok KS, Muller R, Vincent TL, Shefelbine SJ. Multimodal imaging demonstrates concomitant changes in bone and cartilage after destabilisation of the medial meniscus and increased joint laxity. Osteoarthritis Cartilage 2011;19:163–170. [PubMed: 21094262]

29. Bates D, Mächler M, Bolker BM, Walker SC. Fitting linear mixed-effects models using lme4. J. Stat. Softw 2015;67(1):1–48.

30. Chery DR, Han B, Li Q, Zhou Y, Heo SJ, Kwok B, Chandrasekaran P, Wang C, Qin L, Lu XL, Kong D, Enomoto-Iwamoto M, Mauck RL, Han L. Early changes in cartilage pericellular matrix micromechanobiology portend the onset of post-traumatic osteoarthritis. Acta Biomater. 2020;111:267–278. [PubMed: 32428685]

31. Feng X. Chemical and biochemical basis of cell-bone matrix interaction in health and disease. Curr. Chem. Biol 2009;3:189–196. [PubMed: 20161446]

32. Jia H, Ma X, Wei Y, Tong W, Tower RJ, Chandra A, Wang L, Sun Z, Yang Z, Badar F, Zhang K, Tseng WJ, Kramer I, Kneissel M, Xia Y, Liu XS, Wang JHC, Han L, Enomoto-Iwamoto M, Qin L. Loading-induced reduction in Sclerostin as a mechanism of subchondral bone plate sclerosis in mouse knee joints during late-stage osteoarthritis. Arthritis Rheumatol. 2018;70:230–241. [PubMed: 29024567]

33. Felson DT, Gale DR, Elon Gale M, Niu J, Hunter DJ, Goggins J, Lavalley MP. Osteophytes and progression of knee osteoarthritis. Rheumatology (Oxford) 2005;44:100–104. [PubMed: 15381791]

34. Wiberg C, Heinegård D, Wenglén C, Timpl R, Mörgelin M. Biglycan organizes collagen VI into hexagonal-like networks resembling tissue structures. J. Biol. Chem 2002;277:49120–49126. [PubMed: 12354766]

35. Wiberg C, Klatt AR, Wagener R, Paulsson M, Bateman JF, Heinegård D, Mörgelin M. Complexes of matrilin-1 and biglycan or decorin connect collagen VI microfibrils to both collagen II and aggrecan. J. Biol. Chem 2003;278:37698–37704. [PubMed: 12840020]

36. Lv M, Zhou Y, Polson SW, Wan LQ, Wang M, Han L, Wang L, Lu XL. Identification of chondrocyte genes and signaling pathways in response to acute joint inflammation. Sci. Rep 2019;9:93. [PubMed: 30643177]

37. Berendsen AD, Fisher LW, Kilts TM, Owens RT, Robey PG, Gutkind JS, Young MF. Modulation of canonical Wnt signaling by the extracellular matrix component biglycan. Proc. Natl. Acad. Sci. USA 2011;108:17022–17027. [PubMed: 21969569]

38. Xu TS, Bianco P, Fisher LW, Longenecker G, Smith E, Goldstein S, Bonadio J, Boskey A, Heegaard AM, Sommer B, Satomura K, Dominguez P, Zhao CY, Kulkarni AB, Robey PG, Young MF. Targeted disruption of the biglycan gene leads to an osteoporosis-like phenotype in mice. Nat. Genet 1998;20:78–82. [PubMed: 9731537]

39. Corsi A, Xu T, Chen X-D, Boyde A, Liang J, Mankani M, Sommer B, Iozzo RV, Eichstetter I, Robey PG, Bianco P, Young MF. Phenotypic effects of biglycan deficiency are linked to collagen fibril abnormalities, are synergized by decorin deficiency, and mimic Ehlers-Danlos-like changes in bone and other connective tissues. J. Bone Miner. Res 2002;17:1180–1189. [PubMed: 12102052]

40. Miguez PA. Evidence of biglycan structure-function in bone homeostasis and aging. Connect. Tissue Res 2020;61:19–33. [PubMed: 31597498]

41. Hua R, Ni Q, Eliason TD, Y. H, Gu S, Nicolella DP, Wang X, Jiang JX. Biglycan and chondroitin sulfate play pivotal roles in bone toughness via retaining bound water in bone mineral matrix. Matrix Biol. 2020;94:95–109. [PubMed: 33002580]

42. Gronau T, Kruger K, Prein C, Aszodi A, Gronau I, Iozzo RV, Mooren FC, Clausen-Schaumann H, Bertrand J, Pap T, Bruckner P, Dreier R. Forced exercise-induced osteoarthritis is attenuated in mice lacking the small leucine-rich proteoglycan decorin. Ann. Rheum. Dis 2017;76:442–449. [PubMed: 27377816]

43. Nuka S, Zhou W, Henry SP, Gendron CM, Schultz JB, Shinomura T, Johnson J, Wang Y, Keene DR, Ramirez-Solis R, Behringer RR, Young MF, Hoeoek M. Phenotypic characterization of epiphycan-deficient and epiphycan/biglycan double-deficient mice. Osteoarthritis Cartilage 2010;18:88–96. [PubMed: 19932218]

44. Guilak F, Nims RJ, Dicks A, Wu CL, Meulenbelt I. Osteoarthritis as a disease of the cartilage pericellular matrix. Matrix Biol. 2018;71-72:40–50. [PubMed: 29800616]

45. Chery DR, Han B, Zhou Y, Wang C, Adams SM, Chandrasekaran P, Kwok B, Heo S-J, Enomoto-Iwamoto M, Lu XL, Kong D, Iozzo RV, Birk DE, Mauck RL, Han L. Decorin regulates cartilage pericellular matrix micromechanobiology. Matrix Biol. 2021;96:1–17. [PubMed: 33246102]

46. Leiphart RJ, Shetye SS, Weiss SN, Dyment NA, Soslowsky LJ. Induced knockdown of decorin, alone and in tandem with biglycan knockdown, directly increases aged murine patellar tendon viscoelastic properties. J. Biomech. Eng 2020;142:111006. [PubMed: 32766748]

47. Ameye L, Aria D, Jepsen K, Oldberg A, Xu T, Young MF. Abnormal collagen fibrils in tendons of biglycan/fibromodulin-deficient mice lead to gait impairment, ectopic ossification, and osteoarthritis. FASEB J. 2002;16:673–680. [PubMed: 11978731]

48. Carames B, Olmer M, Kiosses WB, Lotz MK. The relationship of autophagy defects to cartilage damage during joint aging in a mouse model. Arthritis Rheumatol. 2015;67:1568–1576. [PubMed: 25708836]

49. Buraschi S, Neill T, Iozzo RV. Decorin is a devouring proteoglycan: remodeling of intracellular catabolism via autophagy and mitophagy. Matrix Biol. 2019;75-76:260–270. [PubMed: 29080840]

50. Poluzzi C, Nastase MV, Zeng-Brouwers J, Roedig H, Hsieh LT, Michaelis JB, Buhl EM, Rezende F, Manavski Y, Bleich A, Boor P, Brandes RP, Pfeilschifter J, Stelzer EHK, Münch C, Dikic I, Brandts C, Iozzo RV, Wygrecka M, Schaefer L. Biglycan evokes autophagy in macrophages via a novel CD44/Toll-like receptor 4 signaling axis in ischemia/reperfusion injury. Kidney Int. 2019;95:540–562. [PubMed: 30712922]
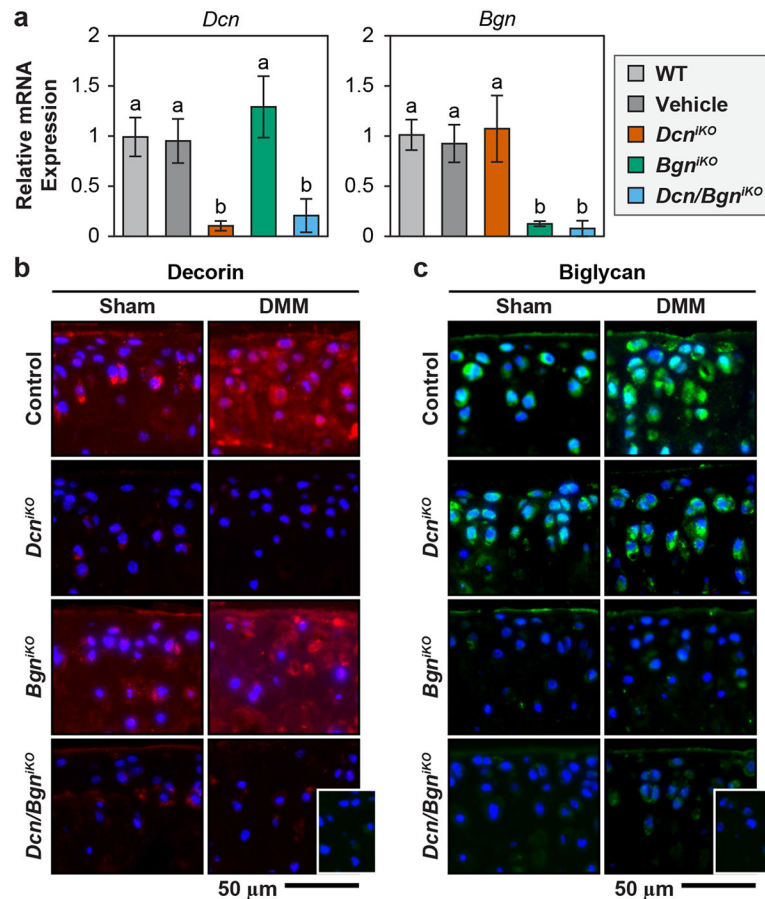
Figure 1.
a) Confirmation of the induced knockout of *Dcn* and/or *Bgn* gene in *Dcn*[iKO] , *Bgn*[iKO] and *Dcn/Bgn*[iKO] mice. In 3-month-old mice, intraperitoneal (i.p.) injection of 3 mg tamoxifen (TM)/40 g body weight for 3 consecutive days reduces the expression of decorin (*Dcn*) and/or biglycan (*Bgn*) to the baseline level by day 5, as measured from femoral head cartilage (mean ± 95% CI, $n = 6$ biological repeats, different letters indicate significant differences between genotypes, $p < 0.001$). Injection of vehicle does not alter the level of *Dcn* or *Bgn* expression relative to the wild-type (WT). In single inducible knockout mice, loss of *Dcn* does not alter the expression of *Bgn*, and vice versa. b,c) Immunofluorescence (IF) images show the reduction of b) decorin and c) biglycan protein content following their respective induced knockout at 8 weeks after DMM and Sham surgeries (inset: negative control, blue: DAPI, $n = 4$).
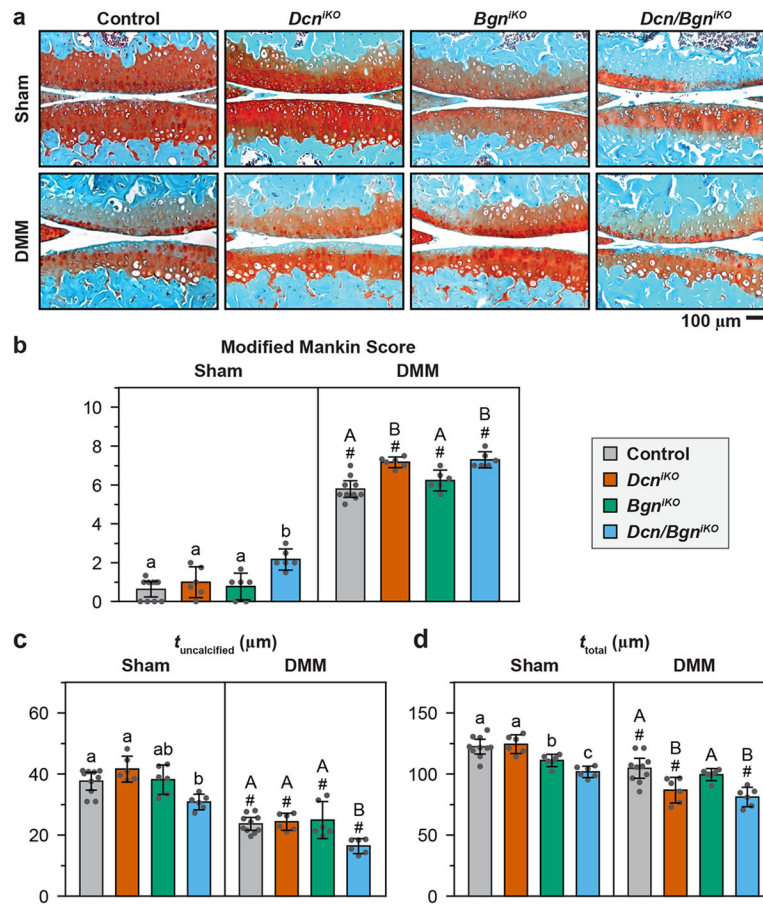
Figure 2.
a) Representative histological images of Safranin O-Fast Green-stained cartilage specimens from control, Dcn^{iKO}, Bgn^{iKO} and Dcn/Bgn^{iKO} mice at 8 weeks after Sham and DMM surgeries, with more severe cartilage damage observed in the Dcn^{iKO} and Dcn/Bgn^{iKO} mice. b) Modified Mankin score and, c) thickness of uncalcified cartilage, $t_{uncalcified}$, and d) thickness of total cartilage, t_{total}, in the medial femur at 8 weeks after Sham and DMM surgeries (mean ± 95% CI, $n = 6$, except $n = 10$ for the control). Each data point represents the value from one animal, different letters indicate significant differences between genotypes for each surgery type, #: $p < 0.05$ between Sham and DMM surgeries for each genotype. Data for Dcn^{iKO} mice are adapted from Ref. [15] with permission.
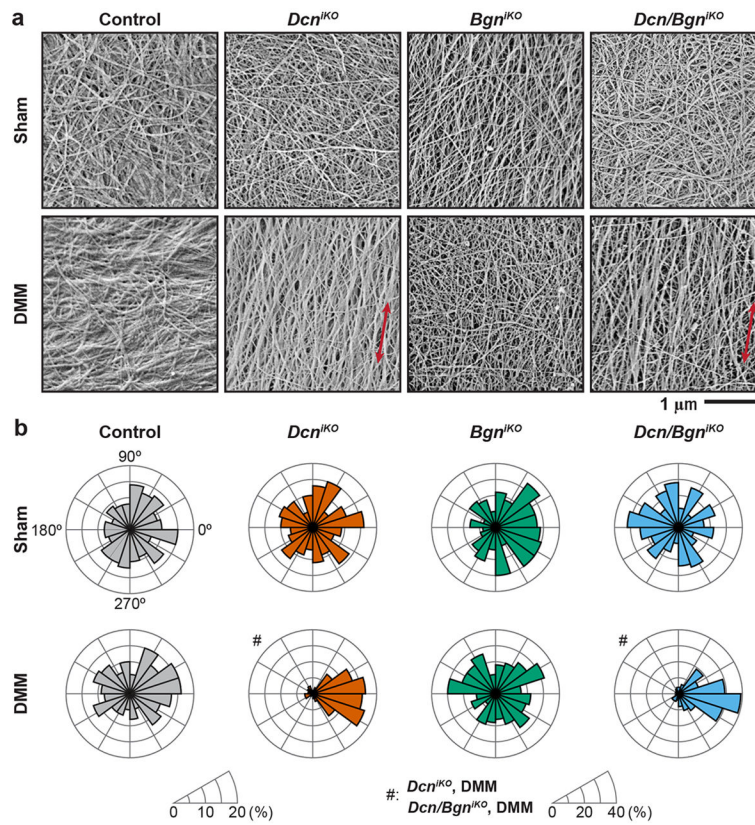
Figure 3.
a) Representative scanning electron microscopy (SEM) images showing the nanostructure of collagen fibrils on condyle cartilage surfaces at 8 weeks after Sham and DMM surgeries. Red arrows denote the mediolateral orientation. b) Comparison of the fibril orientation distributions for all four genotypes after Sham and DMM surgeries. Results are from 300 fibrils pooled from $n = 4$ animals per group following setting the average angle to 0° for each joint. Data for control and Dcn^{iKO} mice in panel a) are adapted from Ref.15 with permission.
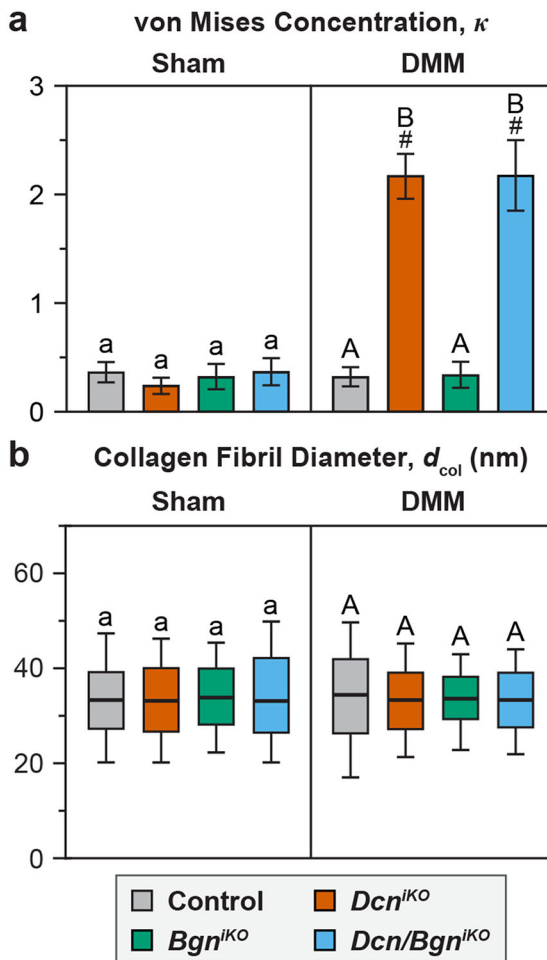
Figure 4.
a) Degree of fibril alignment, as denoted by the von Mises concentration parameter κ, and b) Distribution of collagen fibril diameter, d_{col}, for all four genotypes at 8 weeks after Sham and DMM surgeries. Results are from 300 fibrils pooled from $n = 4$ animals per group. Different letters indicate significant differences between genotypes for each surgery type, [#]: $p < 0.05$ between Sham and DMM surgeries for each genotype. Data for control and Dcn^{iKO} mice in panel a) are adapted from Ref. [15] with permission.
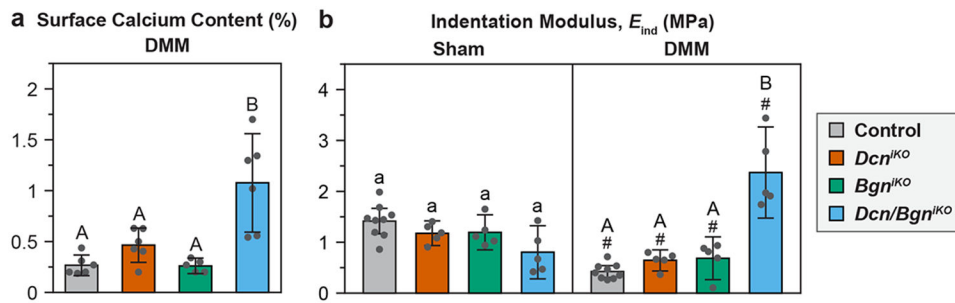
Figure 5.

a) Weight percentage of calcium on the surfaces of condyle cartilage subjected to the DMM surgery, as measured by SEM Energy Dispersive X-ray Spectroscopy (EDS) analysis ($n = 6$, except $n = 5$ for Bgn^{iKO} mice). Each data point represents the averaged value measured from one animal. b) Effective indentation modulus, E_{ind}, of medial condyle cartilage surface, as measured by AFM-nanoindentation ($n = 5$, except $n = 9$ for the control). Each data point represents the average value of 10 locations measured from one joint. Panels b-d: mean ± 95% CI, different letters indicate significant differences between genotypes for each surgery type, #: $p < 0.05$ between Sham and DMM surgeries for each genotype. Data for Dcn^{iKO} mice in panel b) are adapted from Ref. [15] with permission.
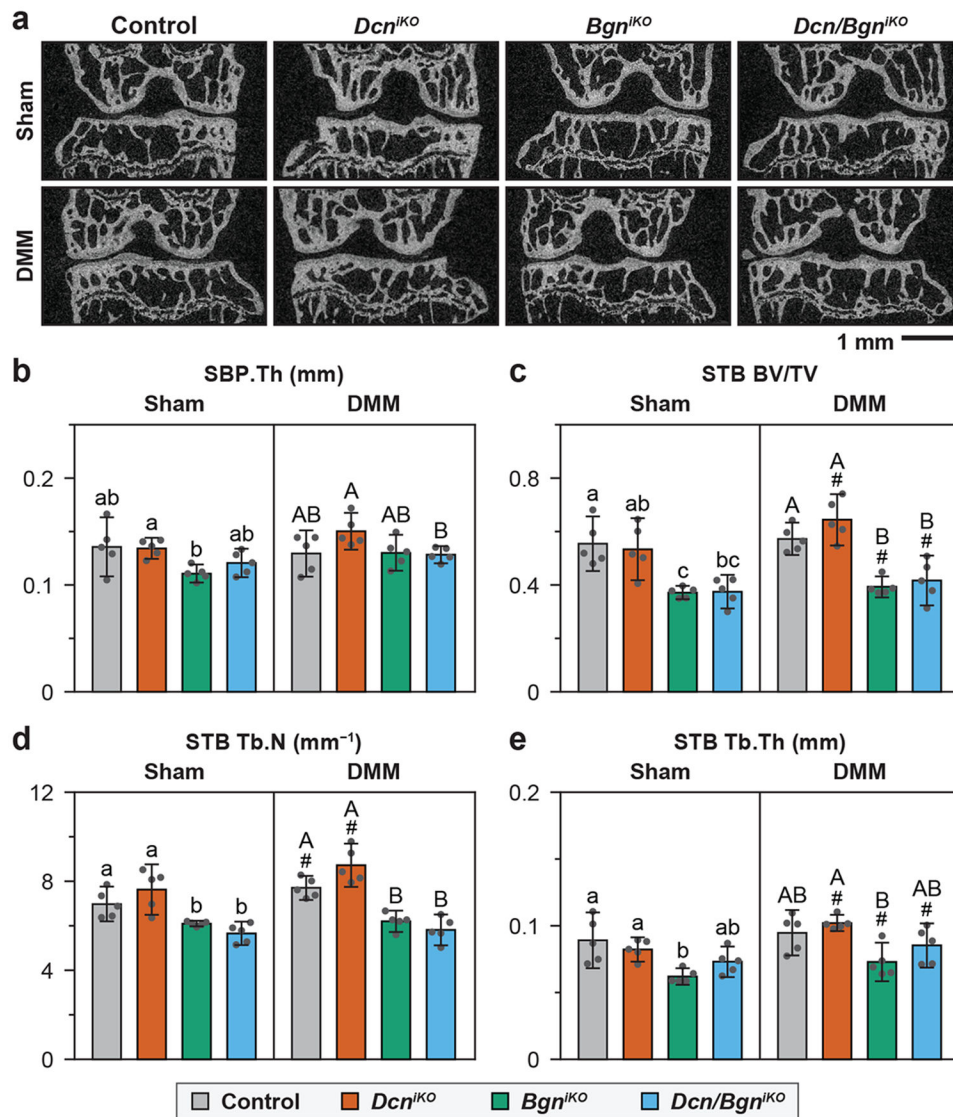
Figure 6.
a) Representative 2D μCT frontal plane images of the knee joint at 8 weeks after Sham and DMM surgeries (L: lateral, M: medial). b) Subchondral bone plate thickness (SBP.Th) and c-e) Subchondral trabecular bone structural parameters, including c) BV/TV: bone volume fraction, d) Tb.N: trabecular number, and e) Tb.Th: trabecular thickness, as measured from the μCT images of medial tibia. Panels b-e: mean ± 95% CI, $n = 5$, each data point represents the averaged value measured from one animal. Different letters indicate significant differences between genotypes for each surgery type, [#]: $p < 0.05$ between Sham and DMM surgeries for each genotype. Data for control and Dcn^{iKO} mice are adapted from Ref. [15] with permission.
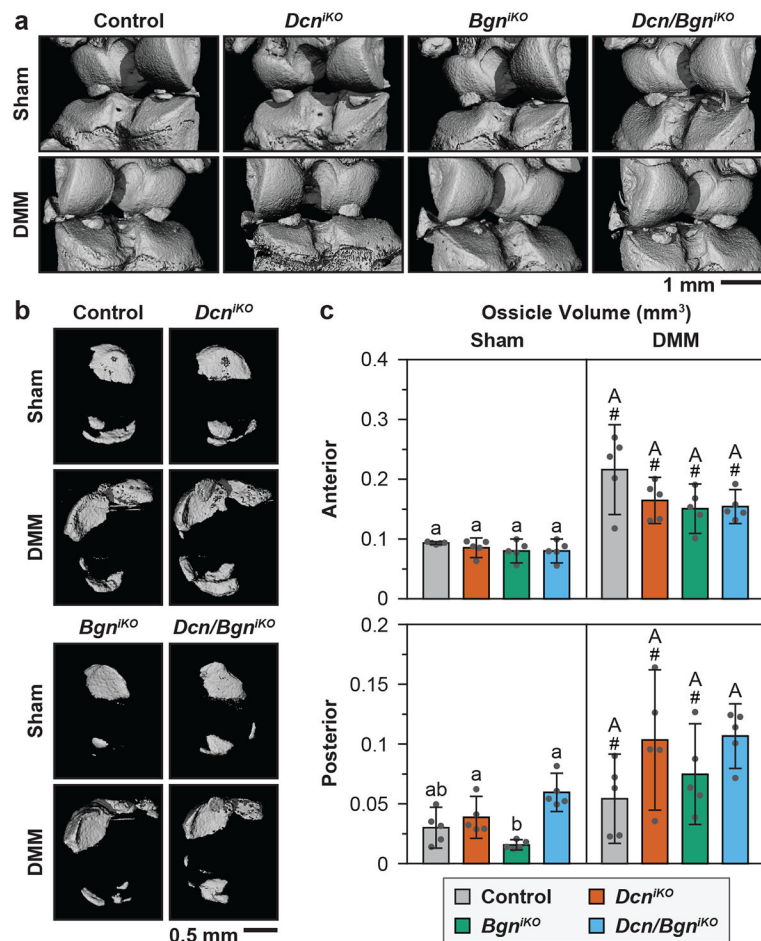
Figure 7.
a) Representative reconstructed 3D μCT images showing the presence of osteophyte in both *Dcn^iKO^* and *Dcn/Bgn^iKO^* joints at 8 weeks after DMM (white arrowheads), but not in other groups. b) Representative reconstructed 3D μCT images (top view) of meniscal ossicles showing increased ossification after DMM for all genotypes. c) Meniscal ossicle volume at both anterior and posterior ends at 8 weeks after Sham and DMM surgeries. Panel c: mean ± 95% CI, $n = 5$, each data point represents the averaged value measured from one animal. Different letters indicate significant differences between genotypes for each surgery type, #: $p < 0.05$ between Sham and DMM surgeries for each genotype. Data for control and *Dcn^iKO^* mice are adapted from Ref. [15] with permission.